

# Neptune Trojans as a Testbed for Planet Formation

E. I. Chiang<sup>1,2</sup> & Y. Lithwick<sup>1</sup>

echiang@astron.berkeley.edu

## ABSTRACT

The problem of accretion in the Trojan 1:1 resonance is akin to the standard problem of planet formation, transplanted from a star-centered disk to a disk centered on the Lagrange point. The newly discovered class of Neptune Trojans promises to test theories of planet formation by coagulation. Neptune Trojans resembling the prototype 2001 QR<sub>322</sub> (“QR”)—whose radius of  $\sim 100$  km is comparable to that of the largest Jupiter Trojan—may outnumber their Jovian counterparts by a factor of  $\sim 10$ . We develop and test three theories for the origin of large Neptune Trojans: pull-down capture, direct collisional emplacement, and *in situ* accretion. These theories are staged after Neptune’s orbit anneals: after dynamical friction eliminates any large orbital eccentricity and after the planet ceases to migrate. We discover that seeding the 1:1 resonance with debris from planetesimal collisions and having the seed particles accrete *in situ* naturally reproduces the inferred number of QR-sized Trojans. We analyze accretion in the Trojan sub-disk by applying the two-groups method, accounting for kinematics specific to the resonance. We find that a Trojan sub-disk comprising decimeter-sized seed particles and having a surface density  $\sim 10^{-3}$  that of the local minimum-mass disk produces  $\sim 10$  QR-sized objects in  $\sim 1$  Gyr, in accord with observation. Further growth is halted by collisional diffusion of seed particles out of resonance. In our picture, the number and sizes of the largest Neptune Trojans represent the unadulterated outcome of dispersion-dominated, oligarchic accretion. Large Neptune Trojans, perhaps the most newly accreted objects in our Solar System, may today have a dispersion in orbital inclination of less than  $\sim 10$  degrees, despite the existence of niches of stability at higher inclinations. Such a vertically thin disk, born of a dynamically cold environment necessary for accretion, and raised in minimal contact with external perturbations, contrasts with the thick disks of other minor body belts.

---

<sup>1</sup>Astronomy Department, University of California at Berkeley, Berkeley, CA 94720, USA

<sup>2</sup>Alfred P. Sloan Research Fellow

*Subject headings:* Kuiper Belt — minor planets, asteroids — solar system: formation — accretion, accretion disks — celestial mechanics — planets and satellites: individual (Neptune)

## 1. INTRODUCTION

Trojans are planetesimals that trace tadpole-shaped trajectories around one of two triangular equilibrium points (Lagrange points) established by their host planet (Lagrange 1873; Murray & Dermott 1999). They are said to inhabit the 1:1 resonance because they execute one orbit about the Sun for every orbit that their host planet makes, staying an average of  $\sim 60^\circ$  forwards or backwards of the planet’s orbital longitude. The Lagrange points represent potential maxima in the frame rotating with the planet’s mean orbital frequency. The Coriolis force renders Trojan motion dynamically stable, while dissipative forces (such as introduced by inter-Trojan collisions) that reduce the energy in the rotating frame cause Trojans to drift from their potential maxima and to escape the resonance.<sup>1</sup> Best known are the Jupiter Trojans: two clouds of rocky, icy bodies that flank the gas giant and whose sizes range up to that of (624) Hektor, which has a characteristic radius  $R \sim 100$  km (Barucci et al. 2002; Marzari et al. 2002; Jewitt, Sheppard, & Porco 2004). The number of kilometer-sized Jupiter Trojans may exceed that of similarly sized Main Belt asteroids (Jewitt, Trujillo, & Luu 2000).

Recently, the first Neptune Trojan, 2001 QR<sub>322</sub> (hereafter “QR”), was discovered by the Deep Ecliptic Survey (DES), an observational reconnaissance of the Kuiper belt at optical wavelengths (Chiang et al. 2003, hereafter C03). This Hektor-sized object librates (oscillates) about Neptune’s forward Lagrange (L4) point and vindicates long-standing theoretical beliefs in the dynamical stability of Neptune Trojans (Holman & Wisdom 1993; Nesvorný & Dones 2002). Billion-year-long orbital integrations of possible trajectories of QR robustly indicate stability and suggest that the object has inhabited the 1:1 resonance for the age of the Solar System,  $t_{\text{sol}} \approx 4.6 \times 10^9$  yr (C03; Marzari, Tricarico, & Scholl 2003; Brasser et al. 2004). Extrapolation of the total population of Neptune Trojans based on the amount of sky surveyed by the DES indicates that Neptune Trojans resembling QR may be 10–30 times as numerous as their Jovian counterparts (C03). If so, their surface mass density would

---

<sup>1</sup>For this reason, Trojan motion is sometimes referred to as dynamically stable but secularly unstable. We will account explicitly for various forms of secular instability experienced by Trojans in §6.

approach that of the current main Kuiper belt to within a factor of a few [e.g., Bernstein et al. 2004; see also equations (24) and (25) of this paper].

Here we investigate the origin of Neptune Trojans. Unlike other resonant Kuiper belt objects (3:2, 2:1, 5:2, etc.) whose existence may be explained by the outward migration of Neptune in the primordial disk of planetesimals and concomitant resonance trapping (Malhotra 1995; Chiang & Jordan 2002; Murray-Clay & Chiang 2004), Neptune Trojans do not owe their genesis to migration. As a planet migrates on timescales much longer than the local orbital period, it scatters neighboring planetesimals onto extremely elongated and inclined orbits by repeated close encounters (C03; Gomes 2003). Such scattering might explain the large velocity dispersions—eccentricities and inclinations with respect to the invariable plane ranging up to  $\sim 0.2$  and  $\sim 0.5$  rad, respectively—observed in the main Kuiper belt today (see, e.g., Elliot et al. 2005; Gomes 2003). By contrast, the orbit of QR is nearly circular and nearly co-planar with the invariable plane; its eccentricity and inclination are  $\sim 0.03$  and  $\sim 0.02$  rad, respectively. In simulations of migration and resonance trapping executed by C03, the sweeping 1:1 resonance fails to trap a single test particle. Instead, Neptune’s migration may destabilize Neptune Trojans. Passage of Neptune Trojans through sweeping secondary resonances with Uranus and the other giant planets can reduce the Trojan population by nearly 2 orders of magnitude (Gomes 1998; Kortenkamp, Malhotra, & Michtchenko 2004).

Do Jupiter Trojans offer any insight into the formation of Neptune Trojans? Morbidelli et al. (2004) propose that in the early planetesimal disk, Jupiter Trojans are captured as Jupiter and Saturn migrate divergently across their mutual 2:1 resonance (see also Chiang 2003 for a more general discussion of divergent resonance crossings). While Jupiter and Saturn occupy the 2:1 resonance, Jupiter’s 1:1 resonance is unstable; planetesimals stream through Trojan libration regions on orbits that tend to be highly inclined due to planetary perturbations. Once the planets depart the 2:1 resonance, stability returns to the 1:1 resonance. At this moment, planetesimals that happen to be passing through Trojan libration regions are trapped there, effectively instantaneously. This “freeze-in” scenario promises to explain the large orbital inclinations—up to  $\sim 0.6$  rad—exhibited by Jupiter Trojans, in addition to Saturn’s observed orbital eccentricity of  $\sim 0.05$  which might result from the planets’ resonance crossing. While we cannot rule out that Neptune Trojans did not also form by freeze-in, analogous motivating observations are absent: The orbital inclination of QR is low; divergent crossing of the 2:1 resonance by Uranus and Neptune may cause Neptune’s eccentricity to exceed its observed value of  $\sim 0.01$  by a factor of  $\sim 3$ ; and finally, the stability of Plutinos and other resonantly trapped Kuiper belt objects is threatened by planetary resonance crossing (Gomes 2001).

Another motivation for studying Neptune Trojans is to infer the formation environment of the host ice giant. Neptune’s formation is the subject of substantial current research because traditional estimates of the planet’s accretion timescale are untenably longer than  $t_{\text{sol}}$  (Thommes, Levison, & Duncan 1999; Goldreich, Lithwick, & Sari 2004, hereafter GLS04). As planetesimals that share Neptune’s orbit, Neptune Trojans may hold clues as to how their host planet assembled. Their composition probably reflects that of Neptune’s rock/ice interior.

We quantitatively develop and assess the viability of three theories for the origin of QR-like objects:

1. Pull-down capture, whereby mass accretion of the host planet converts a planetesimal’s orbit into tadpole-type libration.
2. Direct collisional emplacement, whereby initially non-resonant, QR-sized objects are diverted into 1:1 resonance by physical collisions.
3. *In situ* accretion, whereby QR-sized bodies form by accretion of much smaller seed particles comprising a Trojan sub-disk in the solar nebula. Seed particles are presumed to be inserted into resonance as debris from collisions between planetesimals. The problem of accretion in the Trojan sub-disk is akin to the standard problem of planet formation, transplanted from the usual heliocentric setting to an L4/L5-centric environment.

Peale (1993) analyzes trapping of Jupiter Trojans by nebular gas drag. We do not consider gas dynamics since the outer Solar System after the time of Neptune’s formation was gas-depleted, almost certainly due to photo-evaporation by ultraviolet radiation from the young Sun (e.g., Matsuyama, Johnstone, & Hartmann 2003, and references therein). By mass, Neptune comprises only  $\sim 4\text{--}18\%$  hydrogen and helium (Lodders & Fegley 1998).

While the three mechanisms we examine are not mutually exclusive, the requirements and predictions that each makes independent of the others differ. Faced with only a single known example of a Neptune Trojan and limited data concerning its physical properties, we wield order-of-magnitude physics as our weapon of choice. Many of our simple estimates prove surprisingly illuminating.

In §2, we review the collisionless dynamics of Trojans and supply relations and terminology that will be used in remaining sections. Observed and theoretically inferred properties of Neptune Trojans requiring explanation are listed in §3. There, we also place the birth of Neptune Trojans on the time-line of Neptune’s formation and orbital evolution. In §4,

we argue against pull-down capture as the primary channel for formation. In §5, we quantify and assess the plausibility of demands that direct collisional emplacement places on the planetesimal disk. In §6, we demonstrate how *in situ* accretion can correctly reproduce the inferred number of QR-sized Neptune Trojans. In §7, we summarize our findings and point out directions for future observational and theoretical work.

## 2. BASIC TROJAN MOTION

We review the motions of Trojans hosted by a planet on a circular orbit to establish simple relations used throughout this paper. Some of the material in this section is derived in standard textbooks (e.g., Murray & Dermott 1999). Exceptions include Trojan-Trojan relative motion and the variation of libration period with tadpole size, topics that we develop ourselves.

### 2.1. Epicyclic Motion

Figure 1 illustrates QR’s trajectory: a combination of epicyclic and guiding center motion in the frame co-rotating with the planet. The Trojan completes each ellipse-shaped epicycle (“corkscrew turn”) in an orbit time,

$$t_{\text{orb}} = \frac{2\pi}{\Omega} \approx \frac{2\pi}{\Omega_p} \approx 160 \text{ yr}, \quad (1)$$

where  $\Omega$  and  $\Omega_p$  are the object’s and the host planet’s orbital angular frequencies, respectively. Projected onto the host planet’s orbit plane, the epicycle’s major and minor axes align with the azimuthal and radial directions, respectively. The ratio of semi-axis lengths is  $2ea : ea$ , where  $e$  and  $a \approx a_p$  are, respectively, the osculating eccentricity and orbital semi-major axis of the Trojan, and  $a_p$  is the orbital semi-major axis of the host planet.

### 2.2. Guiding Center Motion

The guiding center of the epicycle loops around the Lagrange point every libration period,

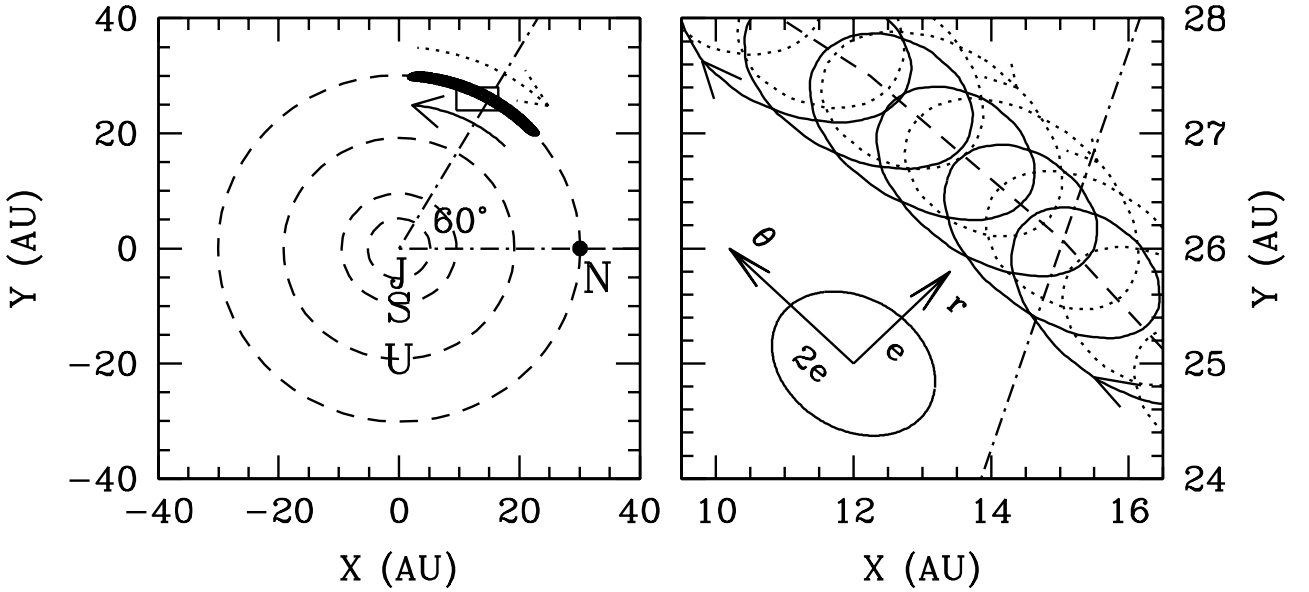


Fig. 1.— Trajectory of the Neptune Trojan, 2001 QR<sub>322</sub> (“QR”), numerically integrated in the presence of the giant planets (denoted J, S, U, N) for  $10^4$  yr and viewed from above the plane of the Solar System. In the left-hand panel, the tube of densely packed points traces QR’s trajectory; the Sun sits at the origin, the distance of each point from the origin equals QR’s instantaneous heliocentric distance, and the angle that the Sun-QR vector makes with respect to the X-axis equals the instantaneous angle between the Sun-QR and Sun-Neptune vectors. The inset box is magnified in the right-hand panel, which shows individual epicycles and their relative dimensions in the radial and azimuthal directions. Each epicycle completes in  $t_{\text{orb}} = 2\pi/\Omega \approx 160$  yr, while the guiding center of the epicycle loops around L4 every  $t_{\text{lib}} \approx 8.9 \times 10^3$  yr. Arrows in both panels indicate directions of motion.

$$t_{\text{lib}} \approx \left( \frac{4}{27\mu} \right)^{1/2} t_{\text{orb}} \approx 8.9 \times 10^3 \text{ yr}, \quad (2)$$

where  $\mu = M_{\text{N}}/M_{\odot} \approx 5 \times 10^{-5}$  is the ratio of Neptune’s mass to the Sun’s. This analytic expression for  $t_{\text{lib}}$  is given by linear stability analysis and is independent of the size of the guiding center orbit. We supply a more precise formula that depends on orbit size in §2.4. The guiding center traces approximately an extremely elongated ellipse (“tadpole”) centered on the Lagrange point and having a radial : azimuthal aspect ratio of  $(3\mu)^{1/2} : 1$ , as depicted in Figure 2. The semi-minor axis of the largest possible tadpole has a length of

$$\max(\delta a) \approx \left( \frac{8\mu}{3} \right)^{1/2} a_{\text{p}}. \quad (3)$$

This length equals the greatest possible difference between the osculating semi-major axes of the Trojan and of the host planet.

### 2.3. Trojan-Trojan Encounters

Consider two Trojans moving initially on pure tadpole orbits with zero epicyclic amplitudes (Figure 2, bottom solid and open circles). A “close” conjunction between the bodies occurs with radial separation  $x$ , at a location away from the turning points of either tadpole orbit and at a time when both bodies are moving in the same direction.<sup>2</sup> The dynamics during the conjunction are, to good approximation, like those of a conjunction between two bodies on circular Keplerian orbits in the absence of the planet. That is, the relative velocity is  $\sim 3\Omega x/2$  and therefore the duration of the encounter is  $\sim 1/\Omega$ . We have verified that this is the case by numerical orbit integrations.

Close conjunctions occur twice per libration period, radially inside and outside the L4 point. We define a synodic time,

$$t_{\text{syn}} \equiv t_{\text{lib}}/2, \quad (4)$$

between successive close conjunctions. Two bodies separated by a radial distance  $x$  and an azimuthal distance  $\lesssim L_{\text{stir}}(x) \equiv 3\Omega x t_{\text{syn}}/2$  undergo close conjunctions every  $t_{\text{syn}}$ .

---

<sup>2</sup>Throughout this paper, we use the word “conjunction” in the usual heliocentric sense; two bodies undergoing a conjunction are collinear with the Sun, and not necessarily with the L4 point.

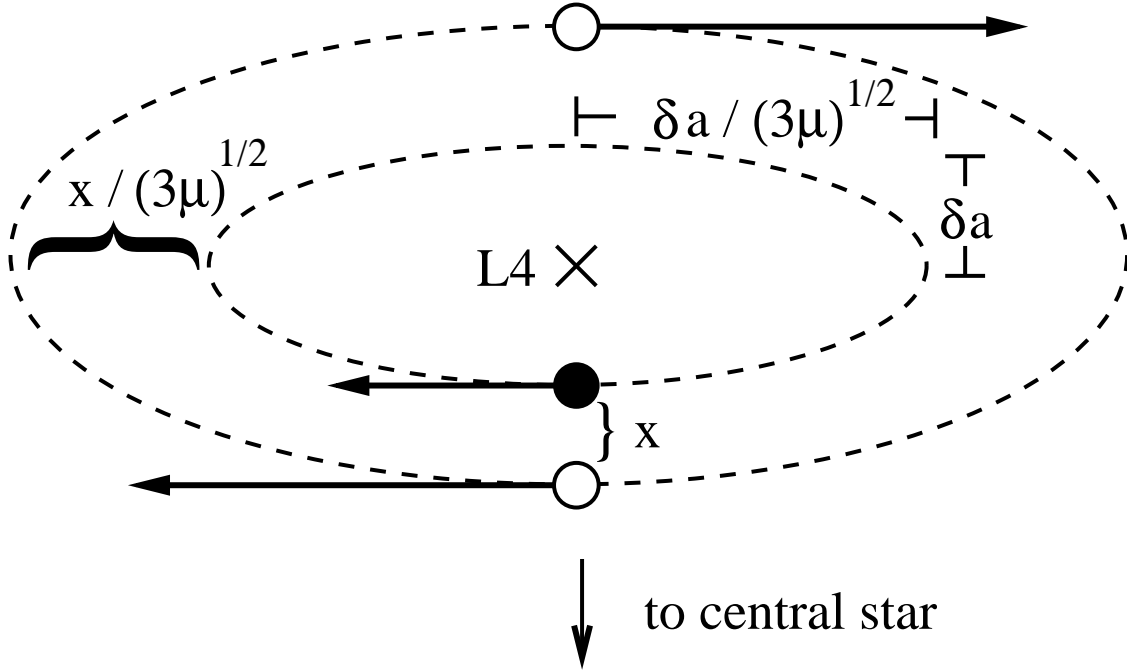


Fig. 2.— Relative motions of orbital guiding centers in Trojan resonance. Each guiding center executes an elliptical trajectory (“tadpole”) around  $L4$  having a radial : azimuthal aspect ratio of  $(3\mu)^{1/2}:1$ . One Trojan (bottom open circle) is shown undergoing a “close” conjunction with another (solid circle). The relative velocity of guiding centers during a close conjunction is given approximately by Keplerian shear. Because bodies are in Trojan resonance, they execute one loop around  $L4$  every  $t_{\text{lib}}$ . Were it not for anharmonic shear, close conjunctions between the two bodies would occur every  $t_{\text{syn}} = t_{\text{lib}}/2$ , alternately above and below  $L4$ . Given anharmonic shear, any given pair of Trojans eventually undergoes “distant” conjunctions, of which one is also shown (top open and solid circles).

## 2.4. Anharmonic Shear

If the libration period,  $t_{\text{lib}}$ , were truly independent of tadpole size, two bodies undergoing close conjunctions would undergo them indefinitely; two conjunctions would occur at the same locations with respect to L4 every libration period.<sup>3</sup> In fact, anharmonicity of the perturbation potential causes the libration period to grow with tadpole size. We calculate numerically the deviation,

$$\delta t_{\text{lib}} \equiv t_{\text{lib}} - t_{\text{lib},0}, \quad (5)$$

as a function of tadpole semi-minor axis,  $\delta a$ , where  $t_{\text{lib},0}$  is the libration period for  $\delta a = 10^{-4}a_{\text{p}}$ . We integrate, via the Burlirsch-Stoer algorithm (Press et al. 1992), test particle orbits having virtually zero epicyclic amplitudes ( $ea \ll \delta a$ ) in the presence of a binary of mass ratio  $\mu = 5 \times 10^{-5}$  and orbital eccentricity  $e_{\text{p}} = 0$ . The numerically computed value of  $t_{\text{lib},0}$  matches that calculated from our analytic expression (2) to within 1 part in  $10^5$ . The result for  $\delta t_{\text{lib}}$ , documented in Figure 3, may be fitted to a power law,

$$\delta t_{\text{lib}} = 0.057 t_{\text{lib},0} \left( \frac{\delta a}{\mu^{1/2} a_{\text{p}}} \right)^{2.0}. \quad (6)$$

The anharmonicity is never strong;  $\delta t_{\text{lib}} < t_{\text{lib}}$ .

This “anharmonic shear” permits phase differences to accumulate between neighboring Trojans. Close conjunctions occur for a finite number of libration periods; eventually, close conjunctions give way to “distant” conjunctions that occur when both bodies are moving in opposite directions on radially opposite sides of L4 (Figure 2, top open and solid circles). Each cycle of close-distant-close conjunctions lasts for a time,

$$t'_{\text{syn}} \approx \left| \frac{d(t_{\text{lib}}^{-1})}{d(\delta a)} x \right|^{-1} \approx 8.8 t_{\text{lib},0} \left( \frac{\mu^{1/2} a_{\text{p}}}{\delta a} \right)^{2.0} \frac{\delta a}{x}, \quad (7)$$

where  $x \ll \delta a$  is the minimum (radial) distance between neighboring tadpole orbits. For a typical value of  $\delta a = 0.5\mu^{1/2}a_{\text{p}}$ , this “grand synodic time” takes a simple form:

$$t'_{\text{syn}} \approx 43 \frac{a_{\text{p}}}{\Omega_{\text{p}} x}, \quad (8)$$

---

<sup>3</sup>Under such a supposition it would nonetheless be incorrect to say that the Trojan libration region is in solid body rotation, since close conjunctions still involve Keplerian shear, as discussed in §2.3.

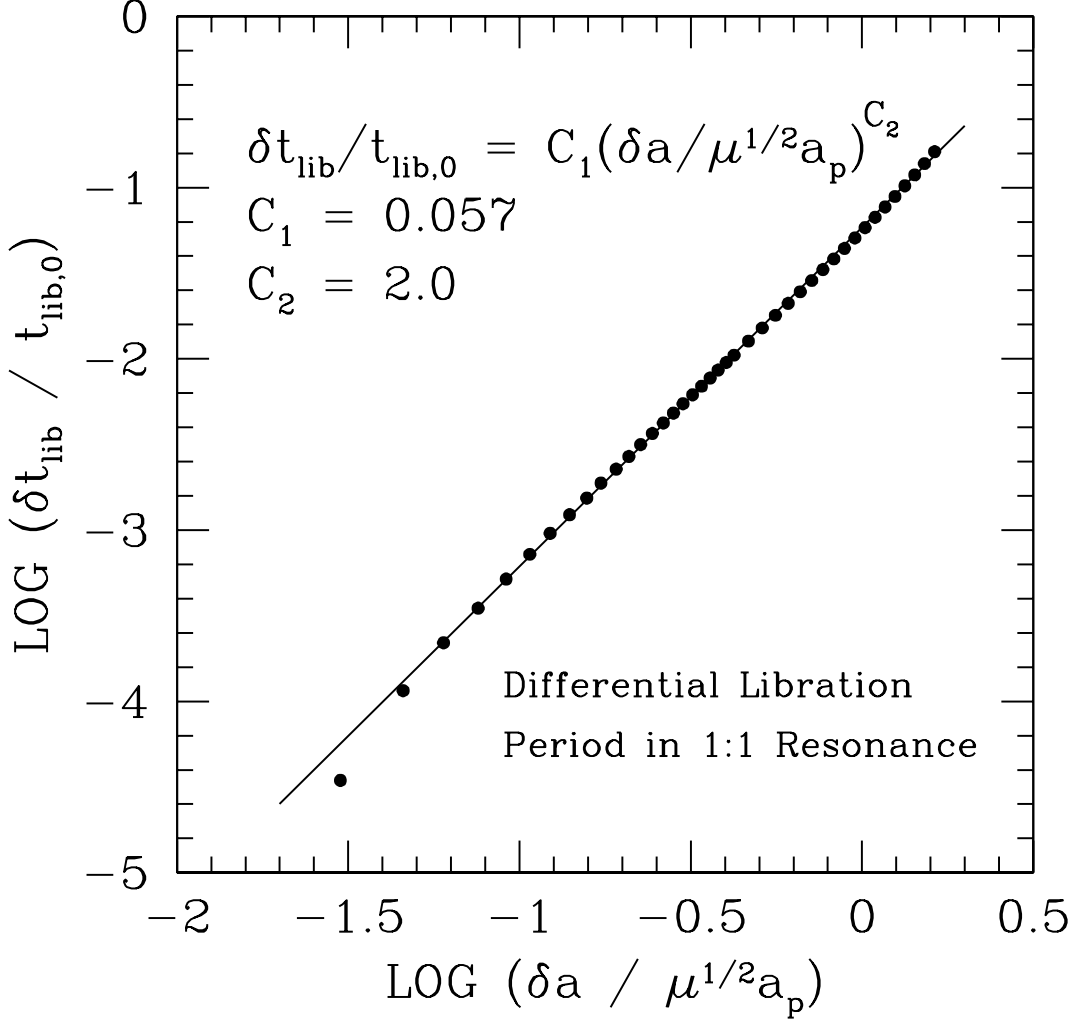


Fig. 3.— Increase of libration period with tadpole size, as measured by numerical integrations of pure tadpole orbits for  $\mu = 5 \times 10^{-5}$  in the circular, restricted, planar 3-body problem. Tadpole size is described by  $\delta a$ , the tadpole semi-minor axis (see Figure 2). As  $\delta a$  increases, the difference,  $\delta t_{\text{lib}}$ , between the measured libration period,  $t_{\text{lib}}$ , and a fiducial libration period,  $t_{\text{lib},0}$  (evaluated at  $\delta a = 10^{-4} a_p$ ), grows. The difference is fitted to a power law (solid line) having the parameters displayed. The increase of libration period with tadpole size (“anharmonic shear”) causes close conjunctions to give way to distant conjunctions over the grand synodic time,  $t'_{\text{syn}}$ .

which is similar to, but of order 10 times longer than, the ordinary synodic time in a circular Keplerian disk away from resonance ( $4\pi a_p/3\Omega_p x$ ).

The time spent undergoing close conjunctions,  $t_{\text{stir}}$ , is shorter than  $t'_{\text{syn}}$  by the ratio of  $L_{\text{stir}}$  to the circumference of a Trojan’s guiding center orbit:

$$t_{\text{stir}} \approx \frac{\pi x}{4 \delta a} t'_{\text{syn}} \approx 56 t_{\text{syn}}, \quad (9)$$

independent of  $x$ . The number of conjunctions that occur during this “stirred” phase is  $t_{\text{stir}}/t_{\text{syn}} \approx 56$ .

## 2.5. Summary

To summarize the behavior described in sections §§2.1–2.4: For a time  $t_{\text{stir}}$ , two neighboring Trojans whose underlying tadpole orbits have semi-minor axes (measured relative to L4) of  $\delta a$  and  $\delta a + x$  undergo close conjunctions. These conjunctions occur every  $t_{\text{syn}} \approx t_{\text{lib}}/2 \approx 4.5 \times 10^3$  yr, and are like ordinary conjunctions between bodies on circular orbits outside of resonance. In particular, an individual conjunction, during which the distance between guiding centers is  $\sim x$ , lasts  $\sim 1/\Omega$ . The number of conjunctions that occur during this stirred phase is typically  $t_{\text{stir}}/t_{\text{syn}} \sim 56$ . After  $t_{\text{stir}}$  time elapses, sufficient phase accumulates between the Trojans that close conjunctions cease. The “unstirred” phase, during which distant conjunctions occur and the distance between bodies is  $\gg x$ , lasts  $t'_{\text{syn}} \sim (\delta a/x)t_{\text{stir}}$ . Afterwards, close conjunctions resume.

## 3. PROPERTIES OF THE NEPTUNE TROJAN POPULATION

We review the properties of Neptune Trojans requiring explanation. With only one Trojan known, we infer many of these characteristics by combining direct observations with theory.

### 3.1. Orbit

Evaluated in a heliocentric, J2000 ecliptic-based coordinate system on Julian date 2451545.0, the osculating elements of QR are  $a = 30.1$  AU,  $e = 0.03$ , and  $i = 0.02$  rad (Elliot et al. 2005). Uncertainties in these values are less than 10% ( $1\sigma$ ) and computed ac-

ording to the procedure developed by Bernstein & Khushalani (2000). The epicycles traced by QR are larger than the radial width of the tadpole;  $e, i > \mu^{1/2} = 0.007$ .

The libration amplitude,

$$\Delta\phi = \max(\lambda - \lambda_p) - \min(\lambda - \lambda_p), \quad (10)$$

equals the full angular extent of the tadpole orbit, where  $\lambda$  and  $\lambda_p$  are the mean orbital longitudes of the Trojan and of the planet, respectively. For QR,  $\Delta\phi \approx 48^\circ$  (C03).

### 3.2. Physical Size

An assumed albedo of 12–4% yields a radius for QR of  $R \sim 65$ –115 km (C03). This size is comparable to that of the largest known Jupiter Trojan, (624) Hektor, whose minimum and maximum semi-axis lengths are  $\sim 75$  km and  $\sim 150$  km, respectively (Barucci et al. 2002).<sup>4</sup> We refer to Trojans resembling QR as “large.”

### 3.3. Current Number

The distribution of DES search fields on the sky, coupled with theoretical maps of the sky density of Neptune Trojans (Nesvorny & Dones 2002), indicate that  $N \sim 10$ –30 large objects (resembling QR) librate about Neptune’s L4 point (C03).

If the true radius of QR is near our estimated lower bound,  $R \sim 65$  km, then the number of large Neptune Trojans is comparable to that of large Jupiter Trojans, of which there are  $\sim 10$  whose radii exceed  $\sim 65$  km (Barucci et al. 2002). If the true radius of QR is closer to our estimated upper bound,  $R \sim 115$  km, then large Neptune Trojans outnumber their Jovian counterparts by a factor of  $\sim 10$ –30, since there is only 1 Jupiter Trojan (Hektor) whose radius exceeds  $\sim 100$  km (Barucci et al. 2002).

### 3.4. Past Number: Collisional Attrition

Large Neptune Trojans observed today are essentially collisionless; they are not the remains of a once greater population that has been reduced in number by collisions. We

---

<sup>4</sup>Hektor might be a near-contact binary (Hartmann & Cruikshank 1978; Tanga et al. 2003).

consider here catastrophic dispersal by collisions with bodies in the same Trojan cloud. By catastrophic dispersal we mean that the mass of the largest post-collision fragment is no greater than half the mass of the original target and that collision fragments disperse without gravitational re-assembly. The lifetimes,  $t_{\text{life}}$ , of large Neptune Trojans against catastrophic dispersal depend on their relative velocities,  $v_{\text{rel}}$ , at impact. If the orbit of QR is typical, then  $v_{\text{rel}} \sim \Omega a \sqrt{e^2 + i^2} \sim 200$  m/s. At such impact velocities, catastrophically dispersing a target of radius  $R \sim 90$  km and corresponding mass  $M$  may be impossible. This is seen as follows. The gravitational binding energy of such a target well exceeds its chemical cohesive energy. Then dispersal requires a projectile mass  $m$  satisfying

$$\frac{f_{\text{KE}}}{2} \left( \frac{mM}{m+M} \right) v_{\text{rel}}^2 \gtrsim \frac{3G(M+m)^2}{5R_{M+m}}, \quad (11)$$

where  $R_{M+m}$  is the radius of the combined mass  $M+m$ , and  $f_{\text{KE}}$  is the fraction of pre-collision translational kinetic energy converted to post-collision translational kinetic energy (evaluated in the center-of-mass frame of  $m$  and  $M$ ). Observed properties of Main Belt asteroid families and laboratory impact experiments suggest  $f_{\text{KE}} \sim 0.01\text{--}0.1$  (Holsapple et al. 2002; Davis et al. 2002). Equation (11) may be re-written

$$\frac{m/M}{(1+m/M)^{8/3}} \gtrsim \frac{8\pi G\rho R^2}{5f_{\text{KE}}v_{\text{rel}}^2}, \quad (12)$$

where  $\rho \sim 2$  g cm<sup>-3</sup> is the internal mass density of an object. For the parameter values cited above, the right-hand-side of equation (12) equals 1.4 (0.1/ $f_{\text{KE}}$ ). Since the maximum of the left-hand-side is only 0.17, catastrophic dispersal cannot occur at such low relative velocities.

Even if the inclination dispersion of Neptune Trojans were instead as large as  $\sim 0.5$  rad—similar to that of Jupiter Trojans, and permitted by dynamical stability studies (Nesvorný & Dones 2002)—collisional lifetimes are probably too long to be significant. Such a large inclination dispersion would imply that  $v_{\text{rel}} \sim 2.7$  km s<sup>-1</sup> and that projectiles having radii  $r \sim 20$  km could catastrophically disperse QR-sized objects [by equation (12)]. The number,  $N_r$ , of such projectiles is unknown. If the size distribution of Neptune Trojans resembles that of Jupiter Trojans (Jewitt et al. 2000), then  $N_r \sim 6000$ , which would imply

$$t_{\text{life}} \sim \frac{4}{\pi} \frac{e_r i_r}{N_r \sqrt{e_r^2 + i_r^2}} \left( \frac{a}{R} \right)^2 \frac{1}{\Omega} \sim 4 \times 10^{11} \left( \frac{6000}{N_r} \right) \left( \frac{90 \text{ km}}{R} \right)^2 \text{ yr} \gg t_{\text{sol}}, \quad (13)$$

where we have taken Trojan projectiles to occupy a volume of azimuthal arclength  $\sim a$ , radial width  $\sim 2e_r a$ , and vertical height  $\sim 2i_r a$ , and inserted  $e_r \approx 0.03$  and  $i_r \approx 0.5$ .

We conclude that the current number of QR-sized Neptune Trojans cannot be explained by appealing to destructive intra-cloud collisions. That large Neptune Trojans have not suffered collisional attrition suggests that their number directly reflects the efficiency of a primordial formation mechanism.

### 3.5. Past Number: Gravitational Attrition

#### 3.5.1. Attrition During the Present Epoch

It seems unlikely that gravitational perturbations exerted by Solar System planets in their current configuration reduced the Neptune Trojan population by orders of magnitude. Nesvorny & Dones (2002) perform the following experiment that suggests Neptune Trojans are generically stable in the present epoch. They synthesize a hypothetical population of 1000 Neptune Trojans by scaling the positions and velocities of actual Jupiter Trojans. Over  $t_{\text{sol}}$ , about 50% of their Neptune Trojans remain in resonance. Objects survive even at high inclination,  $i \sim 0.5$ .

#### 3.5.2. Today’s Trojans Post-Date Neptune’s Final Circularization

By contrast, during the era of planet formation, dramatic re-shaping of the planets’ orbits likely impacted the number of Neptune Trojans significantly. To pinpoint the time of birth of present-day Trojans, we must understand the history of Neptune’s orbit. Current conceptions of this history involve a phase when proto-Neptune’s orbit was strongly perturbed by neighboring protoplanets (GLS04; see also Thommes et al. 1999).<sup>5</sup> Once protoplanets grew to when their mass became comparable to the mass in remaining planetesimals, circularization of the protoplanets’ orbits by dynamical friction with planetesimals was rendered ineffective (GLS04; see also §6). Subsequently, the protoplanets gravitationally scattered themselves onto orbits having eccentricities of order unity. At this time, the mass of an individual protoplanet equaled the isolation mass,

$$M_{\text{iso}} \sim (4\pi A\sigma)^{3/2} a_p^3 (3M_{\odot})^{-1/2} \gtrsim 3M_{\oplus}, \quad (14)$$

---

<sup>5</sup>Our discussion assumes that the ice giant cores formed beyond a heliocentric distance of  $\sim 20$  AU by accreting in the sub-Hill regime (GLS04). Our conclusion that present-day Neptune Trojans formed after Neptune’s orbit finally circularized does not change if we follow instead the scenario in which the ice giant cores were formed between Jupiter and Saturn and were ejected outwards (Thommes et al. 1999).

which is the mass enclosed within each protoplanet’s annular feeding zone of radial width  $\sim 2AR_{\text{H,p}}$ , where  $R_{\text{H,p}} = (M_{\text{iso}}/3M_{\odot})^{1/3}a_{\text{p}}$  is a protoplanet’s Hill sphere radius,  $A \approx 2.5$  (Greenberg et al. 1991), and  $M_{\oplus}$  is an Earth mass. For the surface density,  $\sigma$ , of the protoplanetary disk, we use  $\sigma \gtrsim \sigma_{\text{min}} \sim 0.2 \text{ g/cm}^2$ , where  $\sigma_{\text{min}}$  is the surface density of condensates in the minimum-mass solar nebula at a heliocentric distance of 30 AU. The actual surface density might well have exceeded the minimum-mass value by a factor of  $\sim 3$ , in which case  $M_{\text{iso}} = M_{\text{N}} = 17M_{\oplus}$ . The phase of high eccentricity ended when enough protoplanets were ejected from the Solar System that proto-Neptune’s orbit could once again be kept circular by dynamical friction with planetesimals.

Trojans present prior to Neptune’s high-eccentricity phase would likely have escaped the resonance due to perturbations by neighboring protoplanets. Our numerical integrations show that while Trojans can be hosted by highly eccentric planets, such Trojans undergo fractional excursions in orbital radius as large as those of their hosts, i.e., of order unity (Figure 4). Since fractional separations between protoplanets would only have been of order  $2AR_{\text{H,p}}/a_{\text{p}} \sim 0.1$ , Trojan orbits would have crossed those of nearby protoplanets. Long-term occupancy of the resonance must wait until after protoplanet ejection and the final circularization of Neptune’s orbit.

Note that C03 argue that the existence of Neptune Trojans rules out violent orbital histories for Neptune. We consider their case to be overstated. Present-day Neptune Trojans can be reconciled with prior eccentricities of order unity for Neptune’s orbit, provided that Trojan formation occurs after Neptune’s circularization by dynamical friction.

### 3.5.3. Attrition During the Epoch of Migration

After Neptune’s orbit circularized, the planet may still have migrated radially outwards by scattering ambient planetesimals (Fernandez & Ip 1984; Hahn & Malhotra 1999). Neptune Trojans can escape during migration by passing through secondary resonances with Uranus and the gas giants (Gomes 1998; Kortenkamp, Malhotra, & Michtchenko 2003). In our analysis below, we assume that Trojans form after migration and therefore do not suffer such losses.

## 4. FORMATION BY PULL-DOWN CAPTURE

Trojans can, in principle, be captured via mass growth of the host planet. This mechanism, which we call “pull-down capture,” has been proposed to generate Jupiter Trojans as a

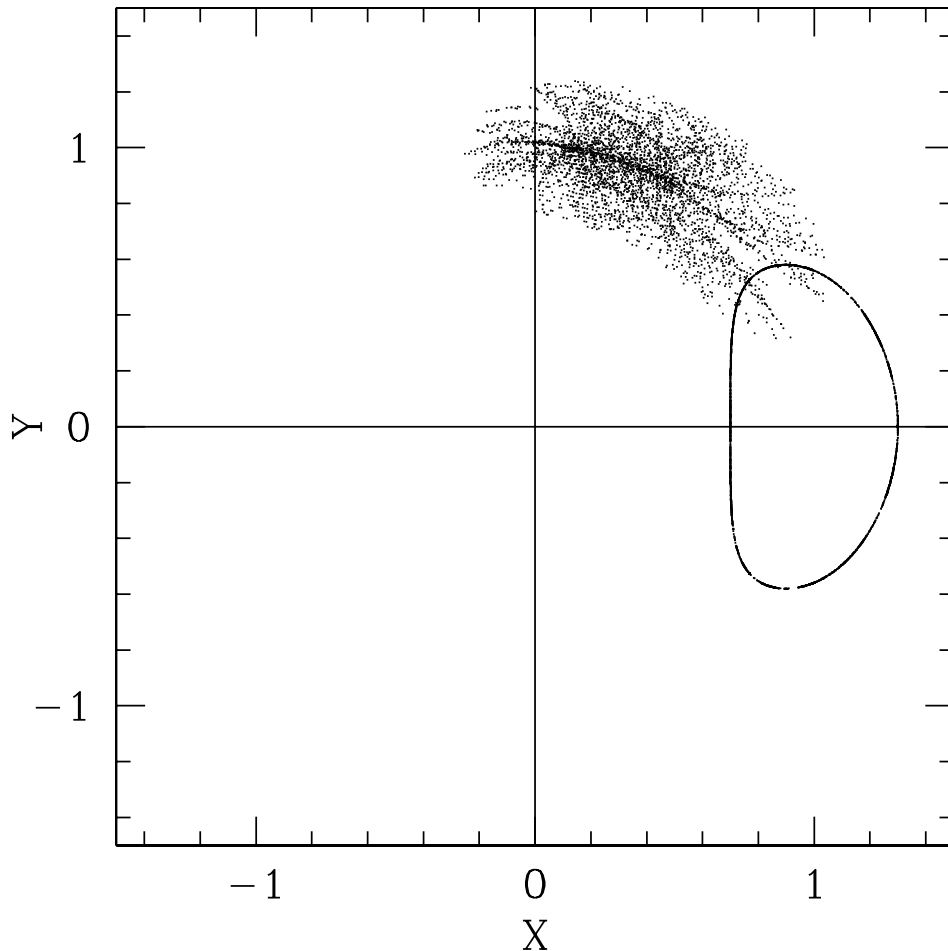


Fig. 4.— Trajectory of a Trojan test particle hosted by a planet ( $\mu = 5 \times 10^{-5}$ ) moving on an orbit of eccentricity  $e_p = 0.3$ . Positions  $X$  and  $Y$  are in units of the semi-major axis of the planet-star binary, and are measured relative to the central star in the frame rotating at the binary mean motion. The planet was initially located at periastron along the  $X$ -axis. Initial conditions for the test particle were such that if  $e_p = 0$ , the test particle would be nearly stationary at L4. Scattered points indicate positions of the Trojan sampled over 1000 orbital periods, while the near-solid curve traces the epicyclic trajectory of the planet. The tadpole region occupied by the Trojan is as radially wide as the planet’s epicycle. Trojan orbits would have crossed those of nearby protoplanets during Neptune’s high eccentricity phase; formation of present-day Neptune Trojans must wait until after Neptune’s orbit finally circularized.

massive gaseous envelope accreted onto the core of proto-Jupiter (Marzari & Scholl 1998ab; Fleming & Hamilton 2000; Marzari et al. 2002).<sup>6</sup>

Pull-down capture may have played a supporting role in the capture of Neptune Trojans, but likely not a leading one. The mechanism operates on the principle of adiabatic invariance. If, as is likely, the mass of the planet grows on a timescale longer than  $t_{\text{lib}}$ , then the libration amplitudes of 1:1 resonators shrink as

$$\Delta\phi \propto \mu^{-1/4}. \quad (15)$$

Horseshoe orbits—those in 1:1 resonance that loop around both triangular points, so that  $\Delta\phi \gtrsim 320^\circ$ —can be converted to Trojan orbits, having  $\Delta\phi \lesssim 160^\circ$ . These bounds derive from the circular, restricted, planar 3-body problem. One shortcoming of current treatments of pull-down capture is that the prior existence of horseshoe librators is assumed without explanation. Horseshoe librators are more unstable than tadpole librators; the former escape resonance more easily due to perturbations by neighboring planets.<sup>7</sup> What sets the number of these weakly bound resonators at the beginning of pull-down scenarios is unclear.

Even if we ignore the problem of having to explain the origin of horseshoe librators, the efficacy of pull-down capture is weak [equation (15)]. The factor by which Neptune increases its mass subsequent to its high-eccentricity phase is  $M_N/M_{\text{iso}} \lesssim 6$  [equation (14)]. Such mass growth implies that pull-down capture, operating alone, produces Trojans having only large libration amplitudes,  $160^\circ \gtrsim \Delta\phi \gtrsim 160^\circ/6^{1/4} \sim 100^\circ$ . By contrast, the orbit of QR is characterized by  $\Delta\phi \approx 48^\circ$ . Excessive libration amplitudes even afflict Jupiter Trojans formed by pull-down capture, despite the  $\sim 30$ -fold increase in Jupiter’s mass due to gas accretion (Marzari & Scholl 1998b). Collisions have been proposed to extend the distribution of libration amplitudes down to smaller values (Marzari & Scholl 1998b), but our analysis in §3.4 indicates that large Trojans are collisionless. Moreover, inter-Trojan collisions dissipate energy and therefore deplete the resonance; see §1 and §6.

In sum, formation of large Neptune Trojans by pull-down capture seems unlikely because libration amplitudes are inadequately damped; Neptune increases its mass by too modest an amount after the planet’s high-eccentricity phase.

---

<sup>6</sup>“Pull-down capture” was coined to describe capture of bodies onto planetocentric (satellite) orbits by mass growth of the planet (Heppenheimer & Porco 1977).

<sup>7</sup>Karlsson (2004) has identified  $\sim 20$  known asteroids that, sometime within 1000 years of the current epoch, occupy horseshoe-like orbits with Jupiter. These objects transition often between resonant and non-resonant motion.

## 5. FORMATION BY DIRECT COLLISIONAL EMPLACEMENT

Large, initially non-resonant objects of radius  $R \sim 90$  km can be deposited directly into Trojan resonance by collisions. Successful deflection of target mass  $M$  by projectile mass  $m$  requires that the post-collision semi-major axis of  $M$  lie within  $\sim \mu^{1/2} a_p$  of  $a_p$ , and that the post-collision eccentricity be small (resembling that of QR). We estimate the number of successful depositions into one Trojan cloud as follows. First, we recognize that successful emplacement requires  $m \sim M$ , since it is difficult for widely varying masses to significantly deflect each other's trajectory. This will be justified quantitatively in §5.1. Each target of mass  $M$  and radius  $R$  collides with

$$U_{\text{col}} \sim n_M R^2 v_M \quad (16)$$

similar bodies per unit time, where

$$n_M \sim \frac{\Sigma_M \Omega_p}{M v_M} \quad (17)$$

is the number density of bodies,  $\Sigma_M$  is their surface density, and  $v_M$  is their velocity dispersion (assumed isotropic). Of the collisions occurring within a heliocentric annulus centered at  $a = a_p$  and of radial width  $\Delta a = a_p/2$ , only a fraction,  $f_{\text{col}}$ , successfully deflect targets onto low eccentricity orbits around one Lagrange point. After time  $t_{\text{col}}$  elapses, the number of successful emplacements into one cloud equals

$$N_{\text{col}} \sim \frac{2\pi \Sigma_M a_p \Delta a}{M} U_{\text{col}} f_{\text{col}} t_{\text{col}} \quad (18)$$

$$\sim \frac{2\pi \Omega_p a_p \Delta a R^2}{M^2} \Sigma_M^2 f_{\text{col}} t_{\text{col}}. \quad (19)$$

In §5.1, we detail our method of computing  $f_{\text{col}}$ . We describe and explain the results of our computations in §5.2. Readers interested only in the consequent demands on  $\Sigma_M$  and  $t_{\text{col}}$  and whether they might be satisfied may skip to §5.3.

### 5.1. Method of Computing $f_{\text{col}}$

For fixed target mass  $M$  and projectile mass  $m$ ,

$$f_{\text{col}} = \frac{1}{\Delta a} \int_{a_p - \Delta a/2}^{a_p + \Delta a/2} f da_M, \quad (20)$$

where  $a_M$  is the pre-collision semi-major axis of mass  $M$ , and  $f$  is the probability that a collision geometry drawn randomly from the distribution of pre-collision orbits yields a successfully emplaced Trojan. We provide a more precise definition of success below. For the collision geometries that we experiment with, we find that  $\Delta a = 0.5a_p$  ensures that all successful collisions are counted (i.e.,  $f$  goes to zero at the limits of integration).

Computing  $f_{\text{col}}$  requires knowing how pre-collision semi-major axes, eccentricities, and inclinations are distributed. Since these distributions in the early Solar System are unknown, we attempt the more practicable goal of estimating the maximum value of  $f_{\text{col}}$  by experimenting with simple cases. To better understand the ingredients for a successful emplacement, we allow  $m \neq M$ . We model collisions as completely inelastic encounters between point particles, though we allow for the possibility of catastrophic dispersal. These simplifications permit maximum deflection of  $M$ 's trajectory and imply that the outcome of a non-catastrophic collision is a merged body of mass  $M + m$ .

We adopt distributions of pre-collision orbital elements as follows. Both  $M$  and  $m$  are taken to have the same distribution of orbital guiding centers (semi-major axes) located outside the planet's Hill sphere. Given input parameter  $B \geq 1$ , semi-major axes of masses  $M$  and  $m$  are uniformly distributed over values greater than  $(1 + B\mu^{1/3})a_p$  and less than  $(1 - B\mu^{1/3})a_p$ , but take no intermediate value. The error incurred in writing equation (18) without regard to the evacuated Hill sphere region is small for  $B\mu^{1/3} < \Delta a/a_p$ . Eccentricities of masses  $M$  are fixed at  $e_M = C\mu^{1/3}$ , and those of masses  $m$  are fixed at  $e_m = D\mu^{1/3}$ , where constants  $C, D \gtrsim B$  to ensure that bodies wander into the Trojan libration zone. Finally, target and projectile are assumed to occupy co-planar orbits. The condition of coplanarity is relaxed in §5.2; for now, we note that allowing for mutual inclination increases the relative velocity at impact and tends to produce catastrophic dispersal and large post-collision eccentricities, reducing  $f_{\text{col}}$ .

Calculations are performed for fixed  $M$  appropriate to  $R = 90$  km and  $\rho = 2$  g cm<sup>-3</sup>. For each  $B, C, D, m, a_M$ , and true anomaly (angular position from pericenter) of mass  $M$ , all possible orbits of  $m$  that collide with  $M$  are computed. This set of possible orbits is labelled by the true anomaly of  $m$  at the time of collision. Post-collision semi-major axes and eccentricities are computed by conserving momentum in the radial and azimuthal directions separately. Successful emplacements involve (a) post-collision semi-major axes of the merged body that lie within  $\pm\mu^{1/2}a_p$  of  $a_p$ ; (b) no catastrophic dispersal, where the criterion for dispersal is given by equation (11) and two values of  $f_{\text{KE}}$  are tested, 0.01 and

0.1; and (c) post-collision eccentricities less than 0.05. This last requirement is motivated by QR’s eccentricity ( $e = 0.03$ ) and the tendency for more eccentric objects to be rendered unstable by Uranus. Successful collisions are tallied over all true anomalies of  $m$  and  $M$ , divided by the total number of collision geometries possible, and divided further by  $2\pi$  to yield  $f$ . The last division by  $2\pi$  accounts for the probability that the collision occurs at the appropriate azimuth relative to Neptune, in an arc of azimuthal extent  $\sim 1$  rad centered on L4. For the small-to-moderate eccentricities considered here, every interval in true anomaly is taken to occur with equal probability.

## 5.2. Results for $f_{\text{col}}$

Families of curves for  $f_{\text{col}}$  as a function of  $m$  are presented in Figures 5 and 6. The figures correspond to two different values of  $f_{\text{KE}}$ , 0.1 and 0.01, respectively. Each curve is labelled by the parameter values  $(B,C,D)$ . The maximum efficiency attainable is  $\max(f_{\text{col}}) \sim 10^{-3}$ , appropriate for  $(B,C,D) = (1,2,2)$  and  $m \approx M$ . Curves for  $(1, 1, 2)$ ,  $(1, 1.5, 1.5)$ , and  $(1, 2, 1)$  are similar to but still slightly below that for  $(1, 2, 2)$  and not shown.

Successful collision geometries are those in which the masses have orbital guiding centers (semi-major axes) on opposite sides of L4. Typically one mass is near the periapse of its orbit, while the other is near apoapse. The maximum efficiency of  $\sim 10^{-3}$  can be rationalized as follows. From our computations, the fraction of time one mass spends near apoapse (at a potential Trojan-forming position) is  $\sim 20^\circ/360^\circ \sim 0.055$ . The fraction of time the other spends near periapse is similar,  $\sim 0.055$ . Therefore given that a collision has occurred, the probability that one mass was near periapse and the other was at apoapse is  $\sim 2 \times (0.055)^2 \sim 0.006$ . The probability that the collision occurred at the correct azimuth relative to Neptune, in an arc of angular extent  $\sim 1$  rad centered on L4, is  $\sim 1/2\pi$ . Therefore the joint probability is  $0.006/2\pi \sim 10^{-3}$ .

The reason why the efficiency curves for  $D < C$  ( $e_m < e_M$ ) lie at  $m > M$  (and vice versa) can be understood by examining collisions that occur exactly at periapse for one mass (say  $m$ ) and exactly at apoapse for the other ( $M$ ):  $a_m(1 - e_m) = a_M(1 + e_M) \approx a_p$ . In a successful collision, the post-collision velocity (now purely azimuthal) nearly equals  $v_p = \Omega_p a_p$ . The pre-collision velocity of mass  $m$  is  $v_m = (1 + e_m)^{1/2} v_p$ , while that of  $M$  is  $v_M = (1 - e_M)^{1/2} v_p$ . Success requires

$$Mv_M + mv_m \approx (M + m)v_p, \tag{21}$$

which we express as

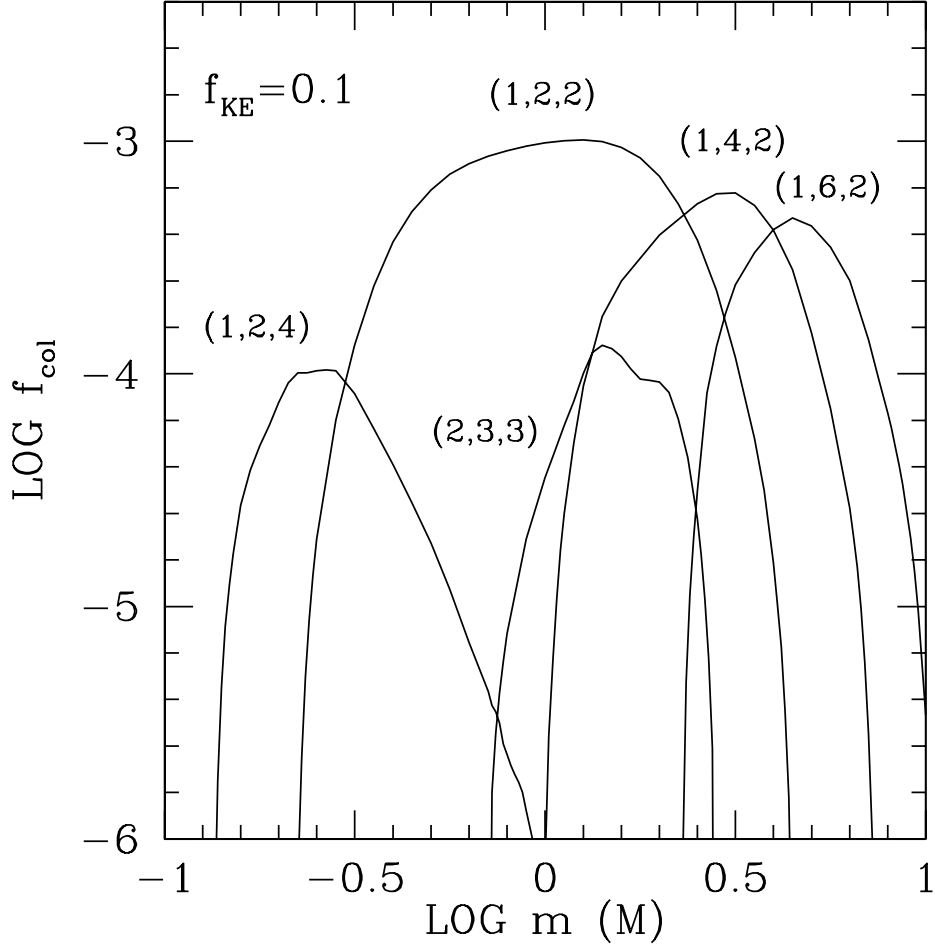


Fig. 5.— Efficiency factors,  $f_{\text{col}}$ , for direct emplacement of QR-sized Trojans by completely inelastic collisions of bodies moving on co-planar orbits. An inelasticity parameter of  $f_{\text{KE}} = 0.1$  is assumed for this figure; see equation (11). Curves are labelled by  $(B,C,D)$ , where  $B$  parameterizes the semi-major axes of pre-collision bodies, and  $C$  and  $D$  parameterize the pre-collision eccentricities of masses  $M$  and  $m$ , respectively. Larger eccentricities and semi-major axes increasingly different from  $a_p$  lead to reduced peak values of  $f_{\text{col}}$ . Curves for  $(1, 1, 2)$ ,  $(1, 1.5, 1.5)$ , and  $(1, 2, 1)$  are similar to but slightly below that for  $(1, 2, 2)$  and not shown.

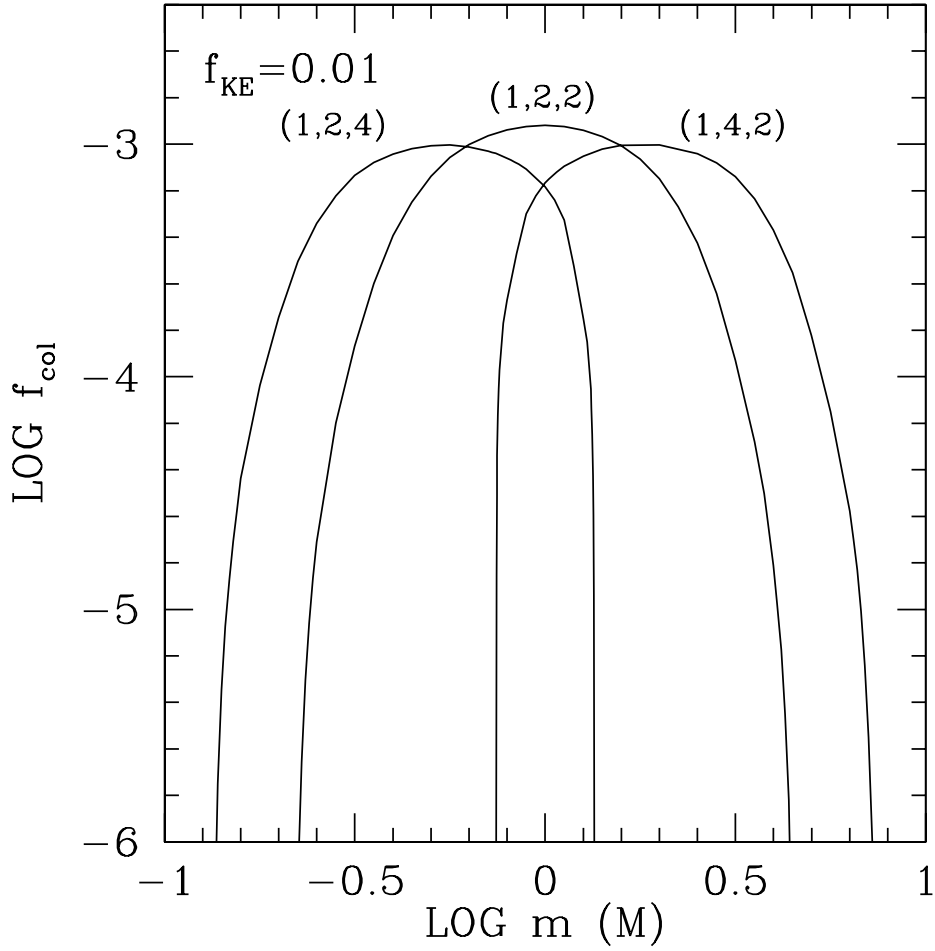


Fig. 6.— Same as Figure 5, except that  $f_{\text{KE}} = 0.01$ , a value so low that catastrophic dispersal is insignificant. Efficiencies are higher than those for  $f_{\text{KE}} = 0.1$  and are symmetric about  $m = M$ .

$$\frac{m}{M+m} \approx \frac{1 - (1 - e_M)^{1/2}}{(1 + e_m)^{1/2} - (1 - e_M)^{1/2}}. \quad (22)$$

Equation (22) implies that  $m \gtrsim M$  for  $e_m \lesssim e_M$ . Similar conclusions obtain if  $m$  and  $M$  collide at their apoapse and periapse, respectively.

In Figure 5, for which  $f_{\text{KE}} = 0.1$ , efficiencies for  $m > M$  are higher than those for  $m < M$  because for fixed  $M$ , large projectile masses  $m$  are more resistant to catastrophic dispersal than small projectile masses: The left-hand-side of equation (12) decreases as  $(m/M)^{-5/3}$  for  $m > M$ , but only as  $m/M$  for  $m < M$ . This asymmetry is not evident in Figure 6, for which  $f_{\text{KE}} = 0.01$ ; catastrophic dispersal is insignificant for such a high inelasticity.

Greater pre-collision eccentricities reduce peak values of  $f_{\text{col}}$  by producing greater relative velocities at impact; these can either lead to catastrophic dispersal or to Trojans having excessive eccentricities.

Removing the assumption of co-planarity has the same effect as increasing pre-collision eccentricities. For example, for  $(B,C,D) = (1,2,2)$ ,  $m/M = 1$ , and  $f_{\text{KE}} = 0.01$ , imposing a relative vertical velocity at the time of collision of  $0.10 \times \Omega_m a_m$ , where  $\Omega_m$  and  $a_m$  are the mean motion and semi-major axis of mass  $m$ , respectively, reduces  $f_{\text{col}}$  from the value shown in Figure 6 by a factor of 10. Imposing a relative velocity of  $0.15 \times \Omega_m a_m$  reduces  $f_{\text{col}}$  to zero; the Trojans deposited all have eccentricities  $> 0.05$ . Successful collisional emplacement is rare for bodies having pre-collision orbital planes that are misaligned by more than  $\sim 6^\circ$ .

While pre-collision orbital planes cannot have a mutual inclination that is large, they still can be substantially inclined with respect to the orbital plane of the planet. Neptune Trojans enjoy dynamical stability at inclinations up to  $\sim 35^\circ$  relative to Neptune’s orbital plane (Nesvorny & Dones 2002).

### 5.3. Final Requirements and Plausibility

Armed with our appreciation for the underlying physics of Neptune Trojan formation by direct collisional emplacement, we re-write equation (19) as

$$\Sigma_M \sim 0.2 \sigma_{\text{min}} \left[ \frac{0.1 t_{\text{sol}}}{t_{\text{col}}} \frac{N_{\text{col}}}{20} \frac{\max(f_{\text{col}})}{f_{\text{col}}} \right]^{1/2} \left( \frac{R}{90 \text{ km}} \right)^2, \quad (23)$$

where  $\sigma_{\text{min}} \sim 0.2 \text{ g/cm}^2$  is the surface density of solids in the minimum-mass nebula at Neptune’s heliocentric distance. The maximum efficiency of  $\max(f_{\text{col}}) \sim 10^{-3}$  is attained for

pre-collision bodies that orbit 1–2 Neptune Hill radii from the planet and whose eccentricities are  $1-2 \times \mu^{1/3} \sim 0.04-0.07$ , i.e., marginally planet-crossing.

The requirements implied by equation (23)—order unity  $\Sigma_M/\sigma_{\min}$  for maximum  $f_{\text{col}}$  and  $t_{\text{col}} \sim 4 \times 10^8$  yr—cannot be met. The efficiency  $f_{\text{col}}$  cannot be maintained at its maximum value for such long  $t_{\text{col}}$ . Large objects within a few Neptune Hill radii of the planet are on strongly chaotic orbits; their eccentricities random walk to values of order unity on timescales much shorter than  $\sim 10^8$  yr. Therefore  $t_{\text{col}} < 0.1t_{\text{sol}}$  and  $f_{\text{col}} < \max(f_{\text{col}})$ , which imply that  $\Sigma_M/\sigma_{\min} > 0.2$ . Such values of  $\Sigma_M/\sigma_{\min}$  introduce a “missing-mass” problem (see, e.g., Morbidelli, Brown, & Levison 2003). Today, in the Kuiper belt at heliocentric distances of  $\sim 45$  AU,  $\Sigma_M/\sigma_{\min} \sim 10^{-3}$  (e.g., Bernstein et al. 2004), where  $\Sigma_M$  is interpreted as the surface density of Kuiper belt objects (KBOs) having sizes  $R \sim 90$  km. If  $\Sigma_M/\sigma_{\min}$  were once greater than order unity—as direct collisional emplacement demands—how its value was thereafter reduced by more than 3 orders of magnitude would need to be explained. One resolution to this problem posits that the number of bodies having  $R \sim 90$  km never exceeded its current low value—that most of the condensates in the local solar nebula instead accreted into smaller, kilometer-sized objects (Kenyon & Luu 1999). Sub-kilometer-sized planetesimals are favored by accretion models for Neptune for their high collision rates and consequent low velocity dispersions (GLS04; see also §6).

To summarize: To collisionally insert  $N_{\text{col}} \sim 20$  QR-sized objects into libration about Neptune’s L4 point requires a reservoir of QR-sized objects having a surface density at least comparable to and possibly greatly exceeding that of the minimum-mass disk of solids. Neither observations of the Kuiper belt nor theoretical models of planetary or KBO accretion support such a picture. We therefore regard the formation of large Neptune Trojans by direct collisional emplacement as implausible.

## 6. FORMATION BY IN SITU ACCRETION

While QR-sized objects are collisionally emplaced with too low a probability, much smaller objects—kilometer-sized planetesimals, for example—may have deposited enough collisional debris into resonance to build the current Trojan population (Shoemaker, Shoemaker, & Wolfe 1989; Ruskol 1990; Peale 1993). Large Neptune Trojans present today might have accreted *in situ* from such small-sized debris.

Modelling the collisional seeding process would require that we understand the full spectrum of sizes and orbital elements of pre-collision bodies, as well as the size and velocity distributions of ejecta fragments. Rather than embark on such a program, we free ourselves

from considerations of the seeding mechanism and instead ask, given a seed population, whether *in situ* accretion is viable at all. We study the dynamics of growth inside the Trojan resonance and quantify its efficiency to constrain the surface density and radii of seed bodies, the number of large Trojans that can form, and the accretion timescale. We will see that *in situ* accretion naturally reproduces the observables with a minimal set of assumptions.

We adopt the two-groups approximation [see, e.g., Goldreich et al. 2004 (GLS04)], in which “big” bodies of radius  $R$ , mass  $M$ , and surface density  $\Sigma$  accrete “small” bodies of radius  $s$ , mass  $m$ , and surface density  $\sigma \gtrsim \Sigma$ . We define

$$g \equiv \sigma/\sigma_{\min} \quad (24)$$

and

$$g_{\min} = \frac{2\pi N\rho R^3}{3\mu^{1/2}a_p^2\sigma_{\min}} = 2 \times 10^{-4}. \quad (25)$$

If  $g = g_{\min}$ , then  $\sigma$  is just sufficient to form  $N = 20$  big bodies of radius  $R = 90$  km out of the Trojan sub-disk of azimuthal length  $a_p$  and radial width  $2\mu^{1/2}a_p$ . Note that  $g = g_{\min}$  does not imply  $\sigma = \sigma_{\min}$ ; the surface density of the Trojan sub-disk may well have been 3 orders of magnitude lower than that of the local minimum-mass disk of condensates.

Small bodies’ epicyclic velocities,  $u$ , are excited by viscous stirring from big bodies and damped by inelastic collisions amongst small bodies. Big bodies’ epicyclic velocities,  $v$ , are excited by viscous stirring from big bodies and damped by dynamical friction with small bodies. A characteristic velocity is

$$v_{\text{H}} \equiv \Omega R_{\text{H}}, \quad (26)$$

the Hill velocity from a big body, where

$$R_{\text{H}} = \left(\frac{M}{3M_{\odot}}\right)^{1/3} a = \frac{R}{\alpha} \quad (27)$$

is the Hill radius of a big body,

$$\alpha \equiv \left(\frac{3\rho_{\odot}}{\rho}\right)^{1/3} \frac{R_{\odot}}{a} \approx 2 \times 10^{-4} \quad (28)$$

is a parameter defined for convenience, and  $\rho_\odot$  and  $R_\odot$  are the average density and radius of the Sun, respectively. Our analysis draws heavily from the pedagogical review of planet formation by GLS04, and the reader is referred there regarding statements that we have not taken the space to prove here.

Any theory of *in situ* accretion must reproduce the observables,  $N \sim 10\text{--}30$  and  $R \sim 90$  km, within the age of the Solar System. A promising guide is provided by the theory of dispersion-dominated, oligarchic planet formation. Conventionally staged in a heliocentric disk, the theory describes how each big body (“oligarch”) gravitationally stirs and feeds from its own annulus of radial half-width  $\sim u/\Omega$ , where  $v_{\text{esc}} > u > v_{\text{H}}$  and  $v_{\text{esc}} \sim v_{\text{H}}/\alpha^{1/2}$  is the escape velocity from a big body.<sup>8</sup> The dominance of each oligarch in its annulus is maintained by runaway accretion. We apply the theory of dispersion-dominated oligarchy to the Trojan sub-disk, recognizing that annuli are now tadpole-shaped and centered on L4, and that the dynamics in the Trojan sub-disk are more complicated than in an ordinary, heliocentric disk because of the cycle of close-distant-close conjunctions (§2). We will need to juggle timescales such as  $t_{\text{lib}}$  and  $t_{\text{stir}}$  that are absent in a non-Trojan environment. Our purpose here is not to survey the entire range of permitted accretion models but to explain how the simplest one works. To this end, we will make assumptions that simplify analysis and permit order-of-magnitude estimation. Many of these assumptions we will justify in §§6.1–6.3. Those that we do not are listed in §6.4.

We derive  $u$  by balancing viscous stirring by big bodies against inelastic collisions with small bodies. We work in the regime where the time between collisions of small bodies,

$$t_{\text{col,u}} \equiv -u \left. \frac{du}{dt} \right|_{\text{col}}^{-1} \sim \frac{\rho s}{\sigma \Omega}, \quad (29)$$

exceeds the grand synodic time,  $t'_{\text{syn,sl}}$ , between a typical small body and its nearest neighboring big body (see §2.4). This choice, which essentially places a lower bound on the small-body sizes  $s$  that we consider, is made so that we may employ simple time-averaged expressions for various rates. We evaluate  $t'_{\text{syn,sl}}$  at  $\delta a = 0.5\mu^{1/2}a$  and  $x = u/\Omega$  [see equation (8)].

The timescale,  $t_{\text{vs,u}}$ , for viscous stirring to double  $u$  is the mean time between close conjunctions of a small body with its nearest neighboring big body, multiplied by the number

---

<sup>8</sup>We do not develop shear-dominated ( $u \lesssim v_{\text{H}}$ ) Trojan oligarchy, because we have discovered that it implicates, for  $g$  not too far above  $g_{\text{min}}$ , seed particles so small that they threaten to rapidly escape resonance by Poynting-Robertson drag.

of conjunctions required for  $u$  to random walk to twice its value. Each conjunction changes  $u$  by  $\Delta u \sim [GM/(u/\Omega)^2]\Omega^{-1} \sim v_{\text{H}}^3/u^2$ . The number of conjunctions required for  $u$  to double is  $(u/\Delta u)^2 \sim (u/v_{\text{H}})^6$ . Since close conjunctions occur at the time-averaged rate of  $(t_{\text{stir}}/t_{\text{syn}})/t'_{\text{syn,sl}} \sim u/a$ , the timescale for viscous stirring to double  $u$  is

$$t_{\text{vs,u}} \equiv u \left. \frac{du}{dt} \right|_{\text{vs}}^{-1} \sim \left( \frac{u}{v_{\text{H}}} \right)^6 \frac{a}{u}. \quad (30)$$

Equating  $t_{\text{vs,u}}$  with  $t_{\text{col,u}}$  gives the equilibrium velocity

$$\frac{u}{v_{\text{H}}} \sim \left( \frac{v_{\text{H}} t_{\text{col,u}}}{a} \right)^{1/5}, \quad (31)$$

valid for  $t_{\text{col,u}} \gtrsim t'_{\text{syn,sl}}$ . The condition  $t_{\text{col,u}} = t'_{\text{syn,sl}}$  implies that

$$\frac{u}{v_{\text{H}}} \approx 43^{1/6} \approx 1.9, \quad (32)$$

independent of  $R$  and  $g$ . We adopt this value for  $u/v_{\text{H}}$  in the remaining discussion. We have assumed that  $u$  approximates the relative velocity between small and big bodies during a conjunction; dynamical friction cooling of big bodies by small bodies ensures that this is the case, as shown in §6.1.

How oligarchic accretion ends determines the final radius,  $R_{\text{final}}$ , of a big body. Oligarchy might end when  $\Sigma \sim \sigma$ . At this stage, big bodies undergo a velocity instability in which viscous stirring overwhelms cooling by dynamical friction and  $v$  runs away (GLS04; §3.5.2; see also §6.1). Larger relative velocities weaken gravitational focussing and slow further growth of big bodies.

There is, however, another way in which oligarchic accretion can end in the Trojan sub-disk: collisional diffusion of small bodies out of resonance. Small bodies can random walk out of the sub-disk before big bodies can accrete them to the point when  $\Sigma \sim \sigma$  (where  $\sigma$  is understood as the original surface density of small bodies, evaluated before loss by diffusion is appreciable). We assume that loss by diffusion halts accretion and check our assumption in §6.2. Changes in the libration amplitudes of big bodies are ignorable, as shown in §6.3. The diffusion time of small bodies is estimated as follows. The orbital guiding centers of small bodies shift radially by about  $\pm u/\Omega$  every  $t_{\text{col,u}}$ . Small bodies random walk out of the resonance over a timescale

$$t_{\text{esc},s} \sim t_{\text{col},u} \left( \frac{\mu^{1/2} a}{u/\Omega} \right)^2, \quad (33)$$

which for our assumption that  $t_{\text{col},u} = t'_{\text{syn},sl}$  equals

$$t_{\text{esc},s} \sim 43 \left( \frac{\alpha a}{R} \right)^3 \left( \frac{v_{\text{H}}}{u} \right)^3 \frac{\mu}{\Omega}. \quad (34)$$

We equate  $t_{\text{esc},s}$  to the assembly time of a big body,  $t_{\text{acc}}$ , to solve for  $R_{\text{final}}$ . Accretion of small bodies to form a big body is accelerated by gravitational focussing, whence<sup>9</sup>

$$t_{\text{acc}} \sim \frac{\rho R}{\sigma \Omega} \left( \frac{u}{v_{\text{esc}}} \right)^2 \sim \frac{\rho R \alpha}{\sigma \Omega} \left( \frac{u}{v_{\text{H}}} \right)^2. \quad (35)$$

Equating  $t_{\text{esc},s}$  to  $t_{\text{acc}}$  yields

$$R = R_{\text{final}} \sim \left( \frac{43 \mu \alpha^2 a^3 \sigma}{\rho} \right)^{1/4} \left( \frac{v_{\text{H}}}{u} \right)^{5/4} \sim 150 \text{ km} \left( \frac{g}{10g_{\text{min}}} \right)^{1/4}. \quad (36)$$

For  $R \sim R_{\text{final}}$ , it follows that

$$t_{\text{acc}} \sim 1 \times 10^9 \left( \frac{10g_{\text{min}}}{g} \right)^{3/4} \text{ yr}, \quad (37)$$

$$u \sim 1.9v_{\text{H}} \sim 2 \left( \frac{g}{10g_{\text{min}}} \right)^{1/4} \text{ m s}^{-1}, \quad (38)$$

$$s \sim 20 \left( \frac{g}{10g_{\text{min}}} \right)^{3/4} \text{ cm}, \quad (39)$$

and that the number of oligarchs accreted equals

$$N_{\text{acc}} \sim \frac{\mu^{1/2} a}{2u/\Omega} \sim 10 \left( \frac{10g_{\text{min}}}{g} \right)^{1/4}. \quad (40)$$

---

<sup>9</sup>Runaway accretion is embodied in equation (35). Consider two oligarchs having radii  $R$  and  $\tilde{R}$ . If the excitation/feeding annuli of the two oligarchs overlap, the bigger oligarch out-accretes the smaller, since  $t_{\text{acc}}/\tilde{t}_{\text{acc}} \sim (R/v_{\text{H}}^2)/(\tilde{R}/\tilde{v}_{\text{H}}^2) \sim \tilde{R}/R$ . This scaling is independent of  $u$  and  $\sigma$  because those variables are common to both competing oligarchs.

We regard (36), (37), and (40) as plausibly explaining the observations: Accretion of decimeter-sized particles having a surface density  $\sim 10$  times that present in QR-sized bodies today generates  $\sim 10$  large Neptune Trojans in  $\sim 1$  Gyr. Their growth naturally halts from the diffusive escape of small bodies out of resonance. Large Neptune Trojans may well be among the most recently assembled bodies in the Solar System.

### 6.1. Checking $v < u$

We have assumed and now check that  $v < u$  so that  $u$  approximates the relative velocity between small and big bodies during a conjunction. Big bodies cool by dynamical friction with small bodies. Since a big body continuously undergoes conjunctions with small bodies in the same manner that it would outside resonance (see §2.3), the standard formula (GLS04) for dynamical friction cooling of big bodies applies:

$$t_{\text{df},v} \equiv -v \left. \frac{dv}{dt} \right|_{\text{df}}^{-1} \sim \frac{\rho R \alpha^2}{\sigma \Omega} \left( \frac{u}{v_{\text{H}}} \right)^4 \sim 7 \times 10^5 \left( \frac{R}{R_{\text{final}}} \right) \left( \frac{10g_{\text{min}}}{g} \right) \left( \frac{u}{1.9v_{\text{H}}} \right)^4 \text{ yr}. \quad (41)$$

To solve for  $v$ , we set this cooling timescale equal to  $t_{\text{vs},v}$ , the timescale for viscous stirring by big bodies to double  $v$ . We exploit the fact that for  $R \sim R_{\text{final}}$ ,  $t_{\text{df},v}$  is of order  $t'_{\text{syn,ll}} \sim 1 \times 10^6 (R_{\text{final}}/R) \text{ yr}$  (the grand synodic time between neighboring big bodies separated by  $x = 2u/\Omega$ ) to derive  $t_{\text{vs},v}$  in the same way that we derived  $t_{\text{vs},u}$ .<sup>10</sup> The key simplification in that derivation was our ability to time-average over the cycle of close-distant-close conjunctions. Each close conjunction between neighboring oligarchs imparts  $\Delta v \sim \Delta u/4 \sim v_{\text{H}}^3/4u^2$ . The number of conjunctions required to double  $v$  is  $(v/\Delta v)^2 \sim 16v^2u^4/v_{\text{H}}^6$ .<sup>11</sup> Since the time-averaged rate of close conjunctions between neighboring big bodies is  $(t_{\text{stir}}/t_{\text{syn}})/t'_{\text{syn,ll}} \sim 2u/a$ ,

$$t_{\text{vs},v} \equiv v \left. \frac{dv}{dt} \right|_{\text{vs}}^{-1} \sim 8 \frac{v^2 u^4 a}{v_{\text{H}}^6 u}. \quad (42)$$

---

<sup>10</sup>When  $R \ll R_{\text{final}}$ ,  $t_{\text{df},v} \ll t'_{\text{syn,ll}}$  and  $v < v_{\text{H}} < u$  whilst the big body is unstirred by its nearest big neighbor, which is the majority of the time.

<sup>11</sup>Our estimate is valid if  $\Delta v < v$ , which in turn demands that  $u/v_{\text{H}} \gtrsim (\pi/6)^{1/6}(\sigma/\Sigma)^{1/6}$ . Physically this means that a given big body is stirred primarily by its nearest big neighbors. This inequality is satisfied for times near  $t_{\text{acc}} \sim t_{\text{esc,s}}$ .

We cast this expression into a form more closely resembling equation (41) by noting that the surface density of big bodies in dispersion-dominated oligarchy is

$$\Sigma \sim \frac{M}{4a(u/\Omega)}, \quad (43)$$

since each big body occupies a feeding annulus of width  $\sim 2u/\Omega$  and perimeter  $\sim 2a$ . Then

$$t_{\text{vs,v}} \sim \frac{8\pi}{3} \frac{\rho R \alpha^2 v^2 u^2}{\Sigma \Omega v_{\text{H}}^4}. \quad (44)$$

Equating  $t_{\text{vs,v}}$  with  $t_{\text{df,v}}$  yields

$$\frac{v}{u} \sim \left( \frac{3}{8\pi} \frac{\Sigma}{\sigma} \right)^{1/2}. \quad (45)$$

Therefore  $v < u$  provided  $\Sigma \lesssim (8\pi/3)\sigma$ ; this inequality is well satisfied while big Trojans grow. Goldreich et al. (2004, GLS04) point out that if  $\Sigma \gtrsim \sigma$ , dynamical friction cooling fails to balance viscous stirring and  $v$  de-stabilizes. Though we agree (to order-of-magnitude) with this conclusion, the power-law index in equation (45) should be  $1/2$ , not  $1/4$  as stated in equation (109) of GLS04. The error arises in GLS04 because these authors assume that epicycles of big bodies overlap; in dispersion-dominated Trojan oligarchy for  $v < u$ , they do not.

## 6.2. Checking that Diffusive Loss Limits Accretion

Our assumption that loss by diffusion of small bodies limits accretion is valid if  $R_{\text{final}} < R_{\text{iso,Trojan}}$ , where the latter radius is that of the isolation mass. In dispersion-dominated oligarchy, the isolation mass is that contained in a tadpole-shaped annulus of perimeter  $\sim 2a_{\text{p}}$  and radial width  $\sim 2u/\Omega$ :

$$\frac{4\pi\rho R_{\text{iso,Trojan}}^3}{3} \sim \frac{4a_{\text{p}}u\sigma}{\Omega}, \quad (46)$$

from which we derive

$$R_{\text{iso,Trojan}} \sim \left( \frac{3a_{\text{p}}\sigma u}{\pi\rho\alpha v_{\text{H}}} \right)^{1/2} \sim 300 \left( \frac{g}{10g_{\text{min}}} \right)^{1/2} \text{ km} > R_{\text{final}}. \quad (47)$$

Thus escape of small bodies by diffusion prevents big bodies from undergoing their last potential radius-doubling. Velocity instability still eventually occurs; but it is triggered by decay of  $\sigma$  by escape of small bodies, not by accretion of big bodies.

### 6.3. Checking that Big Bodies Do Not Migrate

We have assumed that the libration amplitudes of big bodies do not change significantly over the accretion epoch. First we consider how big bodies change the libration amplitude of a big body; the effects of small bodies are considered separately in the latter half of this sub-section. A lower bound on the time it takes a big body to escape the resonance can be established by considering the big bodies to be spaced by  $x = R_H$ . In this case, the semi-major axis of a big body changes by  $\pm R_H$  every time the body undergoes a close conjunction with its nearest neighbor (in other words, the big bodies swap places every close conjunction). Then a big body random walks out of the resonance over a timescale of  $t_{\text{diff,b}} \sim (\mu^{1/2}a/R_H)^2 a/v_H \sim 2 \times 10^8 (150 \text{ km}/R)^3 \text{ yr}$ , where  $\sim a/v_H$  is the time between close conjunctions, time-averaged over the grand synodic period. Though this diffusion time is a factor of 5 shorter than  $t_{\text{acc}} \sim t_{\text{esc,s}} \sim 10^9 \text{ yr}$ , the true escape time of big bodies will be larger than  $t_{\text{diff,b}}$  because the actual epicycles traced by big bodies—and therefore the characteristic stepsizes in any random walk—only approach  $\sim R_H/20$  in size. Crude estimates suggest that the true escape time of big bodies due to interactions with other big bodies is orders of magnitude longer than the above estimate of  $t_{\text{diff,b}}$  for our model parameters.

Viscous stirring by small bodies is much less effective than viscous stirring by big bodies. Since the epicycles of small bodies cross the orbits of big bodies, the timescale for viscous stirring by small bodies to double  $v$  is given by the usual formula

$$t|_{\text{vs,v,s}} \sim \frac{\rho R \alpha^2 M v^2 u^4}{\sigma \Omega m u^2 v_H^4} \quad (48)$$

(GLS04). This timescale is safely longer than that for viscous stirring by big bodies to double  $v$  [equation (44)] by

$$\frac{t|_{\text{vs,v,s}}}{t|_{\text{vs,v}}} \sim \frac{3 \Sigma M}{8\pi \sigma m} \gg 1. \quad (49)$$

Changes in libration amplitudes of big bodies by dynamical friction cooling by small bodies are also ignorable. A big body experiences friction with small bodies inside and outside its tadpole-shaped, guiding center orbit. Interactions with the interior disk of small

bodies will be of the same magnitude as interactions with the exterior disk, differing only by of order  $\epsilon \ll 1$ . Simple estimates suggest that  $\epsilon < 10^{-2}$ . If the surface density of small bodies changes fractionally by order unity from the Lagrange point to the outer edge of the resonance, then  $\epsilon \sim (v/\Omega)/(\mu^{1/2}a) \sim 5 \times 10^{-3}$ . If no such large scale gradient exists,  $\epsilon \sim v/(\Omega a) \sim 4 \times 10^{-5}$ . During each period of distant conjunctions, when small bodies reduce the size of the big body’s epicycle by of order  $v/\Omega$  over the cooling timescale  $t_{\text{df},v}$ , the change to the size of the tadpole orbit will be at most of order  $|\Delta(\delta a)| \sim \epsilon(v/\Omega)$ . Conservatively we assume that the change always has the same sign; that is, the big body suffers a steady drift either towards or away from the Lagrange point at a velocity

$$w_{\text{drift,b}} \sim \frac{\epsilon v/\Omega}{t_{\text{df},v}}. \quad (50)$$

The big body migrates across the width of the resonance over a time

$$t_{\text{drift,b}} \sim \frac{\mu^{1/2}a}{w_{\text{drift,b}}} \sim 1 \times 10^{10} \left( \frac{0.01}{\epsilon} \right) \text{ yr} \quad (51)$$

where we have used  $v \sim u/10$ ,  $u \sim 2 \text{ m/s}$ , and  $t_{\text{df},v} \sim 7 \times 10^5 \text{ yr}$ . Therefore unless  $\epsilon \gg 10^{-2}$ , systematic drifts of a big body can be ignored over  $t_{\text{acc}} \sim t_{\text{esc},s} \sim 10^9 \text{ yr}$ .

#### 6.4. Neglected Effects and Unresolved Issues

In estimating  $u$  and  $v$ , we assumed that the dominant source of velocity excitation during the era of accretion was viscous stirring by large Trojans. Our neglect of velocity excitation by the other giant planets during this early epoch remains to be justified.

The epicyclic velocities,  $v$ , of big bodies considered above do not exceed  $u \sim 2 \text{ m/s}$ , yet today QR’s epicyclic velocity is  $\sim 100 \text{ m/s}$ . Can viscous stirring, unchecked by dynamical friction after the onset of the velocity instability, produce such a large  $v$ ? The answer is no;  $v \sim 100 \text{ m/s}$  is of order  $v_{\text{esc}}$  and producing it would require near-grazing collisions between QR-sized bodies for which the timescale is  $\sim t_{\text{life}} \sim 7 \times 10^{13} \text{ yr}$  (see §3.4). Therefore we appeal instead to velocity excitation by the other giant planets, occurring after the velocity instability, to generate the epicyclic amplitudes observed today. Perturbations due to the  $\nu_{18}$  inclination resonance and other secular resonances (Marzari et al. 2003; Brasser et al. 2004) seem adequate to the task. Our speculation should be straightforward to verify with numerical orbit integrations.

Finally, the two-groups analysis assumes that the sizes of small bodies do not change while big bodies accrete. Future accretion models should incorporate a spectrum of planetesimal sizes to test this assumption.

## 7. SUMMARY AND DIRECTIONS FOR FUTURE WORK

Neptune Trojans represent one of the most recent additions to the Solar System’s inventory of dynamical species [Chiang et al. 2003 (C03)]. In this work, we have systematically reviewed their properties by combining observation with theory. We have further assessed how three theories—pull-down capture, direct collisional emplacement, and *in situ* accretion—fare in explaining these properties. We wish to elucidate the genesis of Neptune Trojans not only to understand this new class of object in and of itself, but also to shed light on the still debated circumstances of formation of the host ice giant [Thommes et al. 1999; C03; Goldreich et al. 2004 (GLS04)]. Insights into the accretion of Trojans in disks surrounding Lagrange points can carry over into the accretion of planets in disks surrounding stars.

We summarize our main findings as follows.

1. Between  $\sim 10$  and  $\sim 30$  objects comparable in size to the Neptune Trojan 2001 QR<sub>322</sub> (QR) are trapped near Neptune’s forward Lagrange (L4) point. Presumably a similar population exists at L5. Numerical orbit integrations suggest these objects have occupied the 1:1 resonance for the age of the Solar System,  $t_{\text{sol}}$ . The characteristic radius of QR ( $R \sim 90$  km) is comparable to that of the largest known Jupiter Trojan, (624) Hektor. As a function of size for  $R \gtrsim 65$  km, Neptune Trojans are at least as numerous as their Jovian counterparts and may outnumber them by a factor of  $\sim 10$ – $30$ . Their surface mass density approaches that of the main Kuiper belt today to within a factor of a few, and is 3–4 orders of magnitude lower than that of the local minimum-mass disk of condensates.
2. The number of large (QR-sized) Neptune Trojans has not been altered by destructive, intra-cloud collisions. Lifetimes against catastrophic dispersal exceed  $t_{\text{sol}}$  by more than 2 orders of magnitude. That large Neptune Trojans are today essentially collisionless suggests that their number directly reflects the efficiency of a primordial formation mechanism.
3. The existence of Neptune Trojans can be reconciled with violent orbital histories of Neptune (Thommes et al. 1999; GLS04), provided that Trojans form after the planet has its orbit circularized. In histories where Neptune’s eccentricity was once of order

unity, final circularization is achieved by dynamical friction with ambient planetesimals. Long-term occupancy of the Trojan resonance is possible after circularization. This point was not recognized by C03. We regard their argument that present-day Neptune Trojans rule out dramatic scattering events for Neptune to be overstated.

4. Pull-down capture, whereby objects are trapped into Trojan resonance by mass growth of the host planet, is unlikely to have been solely responsible for the origin of large Neptune Trojans. Libration amplitudes (i.e., tadpole orbit sizes) are damped by pull-down capture too inefficiently to explain the libration amplitude of QR. Moreover, the present theory is unsatisfactory because it assumes, without explanation, the prior existence of objects on 1:1 horseshoe orbits. The theory fails to specify what determines the number of weakly bound librators at the onset of pull-down capture.
5. A pair of initially non-resonant, QR-sized objects can be diverted onto low-eccentricity Trojan orbits (like that occupied by QR) when they collide near the periape and apoapse of their respective orbits. The greatest efficiencies of direct collisional emplacement are attained for planetesimals that orbit 1–2 Hill radii away from the planet and whose eccentricities are  $1-2 \times \mu^{1/3} \sim 0.04-0.07$ , where  $\mu = 5 \times 10^{-5}$  is the ratio of Neptune’s mass to the Sun’s. Such orbits are strongly chaotic and cannot be maintained over collision timescales. We estimate that actual efficiencies of direct emplacement are so low that a heliocentric disk of QR-like planetesimals can divert  $N_{\text{col}} \sim 20$  of its members into resonance only if the disk’s surface density exceeds  $\sim 20\%$  that of the local minimum-mass disk of solids. Unfortunately, such a large surface density in QR-sized objects is not supported by observations of the Kuiper belt or by theoretical models of how Neptune and Kuiper belt objects accreted. We therefore discount the formation of large Neptune Trojans by direct collisional emplacement.
6. *In situ* accretion of large Neptune Trojans is viable and attractive. We exercised the two-groups approximation to study accretion dynamics within a primordial Trojan sub-disk composed of small seed bodies having sizes  $s \sim 20$  cm and a surface density lower than that of the local minimum-mass disk of condensates by  $g \sim 2 \times 10^{-3}$ . This surface density is 10 times that of the Neptune Trojan sub-disk today (in QR-sized objects). A plausible way to seed the resonance is by planetesimal collisions that insert ejecta fragments into the Trojan libration region. Big bodies accrete small bodies in our model sub-disk to grow to a radius of  $R_{\text{final}} \sim 150$  km over a period of  $t_{\text{acc}} \sim 1 \times 10^9$  yr. Their number at this time is  $N_{\text{acc}} \sim 10$ , as mandated by the rules of dispersion-dominated oligarchy. Collisional diffusion of small bodies out of the resonance naturally halts further growth. Large Neptune Trojans may be the most recently assembled objects in our planetary system.

We have developed the case that the number and sizes of large Neptune Trojans represent an unadulterated imprint of oligarchic accretion inside resonance. Confirmation of this result would support theories of planet formation by accretion of very small particles (GLS04). What future observations or theoretical work might help to develop this picture? Measurement and calculation of the size distribution of Trojans are natural next steps. Perhaps more intriguing is the question of velocity dispersions inside the Neptune Trojan cloud.

Today, the eccentricity and inclination (with respect to the invariable plane) of QR are both about 0.03. The corresponding epicyclic velocities are of order 200 m/s. In contrast, our accretion model requires velocity dispersions  $\lesssim 2$  m/s while big bodies grow. We suspect, but have yet to check, that today’s velocity dispersions are the result of gravitational perturbations exerted by the other giant planets—perturbations unchecked by dynamical friction during the present, non-accretionary epoch. We might expect planetary perturbations to amplify eccentricities and inclinations of Neptune Trojans to values not exceeding  $\sim 0.1$ . This expectation stems from billion-year-long integrations of possible trajectories of QR (Brasser et al. 2004), which reveal that its eccentricity and inclination (with respect to the invariable plane) stay below  $\sim 0.1$ . For some trajectories, the  $\nu_{18}$  resonance is found to raise the inclination of QR to at most  $7^\circ$  (0.12 rad). More typically, the inclination remains below  $\sim 1.6^\circ$  (Brasser et al. 2004). Thus, even though Neptune Trojans can exist at inclinations as high as  $\sim 35^\circ$  (Nesvorný & Dones 2002; Marzari et al. 2003), we see no reason why these niches at high inclination should be occupied. We might expect mutual inclinations between large Neptune Trojans to be less than  $\sim 10^\circ$ . This picture of a “thin disk” contrasts with the “thick disks” of other minor body belts—Jupiter Trojans, Main Belt asteroids, and the Kuiper belt<sup>12</sup>—and reflects the dynamically cold accretionary environment that we have championed. It is subject to observational test.

We thank D. Jewitt, S. Kortenkamp, H. Levison, J. Lovering, R. Malhotra, R. Murray-Clay, R. Sari, and the DES collaboration for helpful discussions. Exchanges with D.J. and H.L. regarding difficulties with pull-down capture were especially motivating. Footnote 11 is due to R. Sari. Simulations of divergent resonance crossing by R. Murray-Clay were helpful in writing the introduction. Our use of the verb “to anneal” in the abstract is inspired by R. Malhotra. We thank the referee, P. Goldreich, for a prompt and thought-provoking report that helped to improve the presentation of this paper. This work was supported by the National Science Foundation and the Alfred P. Sloan Foundation.

---

<sup>12</sup>With the possible exception of the “core” Classical Kuiper belt having inclinations less than  $\sim 4.6$  degrees with respect to their mean plane (Elliot et al. 2005). Like Neptune Trojans, this cold population may also be relatively dynamically pristine.

## REFERENCES

- Barucci, M.A., Cruikshank, D.P., Mottola, S., & Lazzarin, M. 2002, in Asteroids III, eds. W.F. Bottke, Jr., A. Cellino, P. Paolicchi, & R.P. Binzel (Tucson: Univ. Arizona Press), 273
- Bernstein, G., & Khushalani, B. 2000, *AJ*, 120, 3323
- Bernstein, G., et al. 2004, *AJ*, 128, 1364
- Brasser, R., et al. 2004, *MNRAS*, 347, 833
- Chiang, E.I., & Jordan, A.B. 2002, *AJ*, 124, 3430
- Chiang, E.I. 2003, *ApJ*, 584, 465
- Chiang, E.I., et al. 2003, *AJ*, 126, 430 (C03)
- Davis, D.R., et al. 2002, in Asteroids III, eds. W.F. Bottke, Jr., A. Cellino, P. Paolicchi, & R.P. Binzel (Tucson: Univ. Arizona Press), 545
- Elliot, J.L., et al. 2005, *AJ*, 129, 1117
- Fernandez, J.A., & Ip, W.H. 1984, *Icarus*, 58, 109
- Fleming, H.J., & Hamilton, D.P. 2000, *Icarus*, 148, 479
- Goldreich, P., Lithwick, Y., & Sari, R. 2004, *ARA&A*, 614, 497 (GLS04)
- Gomes, R. 1998, *AJ*, 116, 2590
- Gomes, R. 2001, *AJ*, 122, 3485
- Gomes, R. 2003, *Icarus*, 161, 404
- Greenberg, R., Bottke, W.F., Carusi, A., & Valsecchi, G.B. 1991, *Icarus*, 94, 98
- Hahn, J.M., & Malhotra, R. 1999, *AJ*, 117, 304
- Hartmann, W.K., & Cruikshank, D.P. 1978, *Icarus*, 36, 353
- Heppenheimer, T.A., & Porco, C. 1977, *Icarus*, 30, 385
- Holman, M., & Wisdom, J. 1993, *AJ*, 105, 1987
- Holsapple, K., et al. 2002, in Asteroids III, eds. W.F. Bottke, Jr., A. Cellino, P. Paolicchi, & R.P. Binzel (Tucson: Univ. Arizona Press), 443
- Jewitt, D.C., Sheppard, S., & Porco, C. 2004, in Jupiter. The planet, satellites and magnetosphere, eds. F. Bagenal, T.E. Dowling, & W.B. McKinnon (Cambridge: University Press), 263
- Jewitt, D.C., Trujillo, C.A., & Luu, J.X. 2000, *AJ*, 120, 1140

- Karlsson, O. 2004, *Astron. & Astrophys.*, 413, 1153
- Kenyon, S.J., & Luu, J.X. 1999, *AJ*, 118, 1101
- Kortenkamp, S.J., Malhotra, R., & Michtchenko, T. 2004, *Icarus*, 167, 347
- Lagrange, J.-L., 1873, in *Oeuvres de Lagrange*, Tome Sixième, ed. J.-A. Serret (Paris: Gauthiers-Villars), 229
- Lodders, K., & Fegler, B. 1998, *The Planetary Scientist’s Companion* (New York: Oxford University Press)
- Malhotra, R. 1995, *AJ*, 110, 420
- Marzari, F., & Scholl, H. 1998a, *Icarus*, 131, 41
- Marzari, F., & Scholl, H. 1998b, *Astron. & Astrophys.*, 339, 278
- Marzari, F., Scholl, H., Murray, C., & Lagerkvist, C. 2002, in *Asteroids III*, eds. W.F. Bottke, Jr., A. Cellino, P. Paolicchi, & R.P. Binzel (Tucson: Univ. Arizona Press), 725
- Marzari, F., Tricarico, P., & Scholl, H. 2003, *Astron. & Astrophys.*, 410, 725
- Matsuyama, I., Johnstone, D., & Hartmann, L. 2003, *ApJ*, 582, 893
- Morbidelli, A., Brown, M.E., & Levison, H.F. 2003, *Earth, Moon, & Planets* 92, 1
- Morbidelli, A., Levison, H.F., Tsiganis, K., & Gomes, R., AAS DPS meeting #36, abstract #40.03
- Murray, C.D., & Dermott, S.F. 1999, *Solar System Dynamics* (New York: Cambridge University Press)
- Murray-Clay, R.A., & Chiang, E.I. 2005, *ApJ*, 619, 623
- Nesvorny, D., & Dones, L. 2002, *Icarus*, 160, 271
- Peale, S.J. 1993, *Icarus*, 106, 308
- Press, W.H., Teukolsky, S.A., Vetterling, W.T., & Flannery, B.P. 1992, *Numerical Recipes in Fortran. The Art of Scientific Computing* (Cambridge: University Press)
- Ruskol, E.L. 1990, *Astron. Vestnik*, 24, 244 [in Russian]
- Shoemaker, E.M., Shoemaker, C.S., & Wolfe, R.F. 1989, in *Asteroids II*, eds. R.P. Binzel, T. Gehrels, & M.S. Matthews (Tucson: Univ. Arizona Press), 487
- Tanga, P., et al. 2003, *A&A*, 401, 733
- Thommes, E.W., Duncan, M.J., & Levison, H.F. 1999, *Nature*, 402, 635